


Pressure-temperature phase diagram of $\text{CaK}(\text{Fe}_{1-x}\text{Mn}_x)_4\text{As}_4$ ($x = 0.024$)

Li Xiang[Ⓞ],* Mingyu Xu, Sergey L. Bud'ko, and Paul C. Canfield[†]

*Ames Laboratory, US Department of Energy, Iowa State University, Ames, Iowa 50011, USA
and Department of Physics and Astronomy, Iowa State University, Ames, Iowa 50011, USA*

 (Received 22 May 2022; revised 22 August 2022; accepted 19 September 2022; published 10 October 2022)

Resistance measurements on single crystals of $\text{CaK}(\text{Fe}_{1-x}\text{Mn}_x)_4\text{As}_4$ ($x = 0.024$) were performed under hydrostatic pressure up to 5.15 GPa. The pressure dependence of the magnetic and superconducting transition temperatures and that of the superconducting upper critical field are reported. Our results show that upon increasing pressure, the magnetic transition temperature T_N is suppressed, whereas the superconducting transition temperature T_c first increases and then decreases, exhibiting a maximum at a pressure p_c corresponding to the intersection of the $T_N(p)$ and $T_c(p)$ lines. In addition, a minimum in the normalized slope of the superconducting upper critical field as well as a change in the pressure dependence of the inferred superconducting coherence length are observed at p_c , suggesting a difference in the Fermi surface of the paramagnetic and antiferromagnetic states. Finally, $\text{CaK}(\text{Fe}_{1-x}\text{Mn}_x)_4\text{As}_4$ ($x = 0.024$) likely goes through a half-collapsed tetragonal phase transition at ~ 4.3 GPa, further demonstrating that the half-collapsed tetragonal transition pressure in the $\text{CaKFe}_4\text{As}_4$ system is relatively insensitive to transition metal substitution.

DOI: [10.1103/PhysRevB.106.134505](https://doi.org/10.1103/PhysRevB.106.134505)

I. INTRODUCTION

Since their discovery, Fe-based superconductors (Fe-SC) have attract great interest for their unconventional superconductivity as well its interplay with magnetic, structural degrees of freedom [1–5]. The intensively investigated BaFe_2As_2 family shaped the canonical picture of the phase diagram of Fe-SC [5,6]. At ambient pressure, the parent compound is tetragonal and paramagnetic at high temperature. Upon cooling, it goes through a magnetic/structural phase transition to a stripe-type antiferromagnetic, orthorhombic state [6–8]. Upon chemical substitution or physical pressurization, the magnetic/structural transitions are separated and suppressed to lower temperatures and at certain level superconductivity emerges, often in a dome-like region with the magnetic/structural ordering line intersecting the T_c dome near its maximal value [5,9–12].

Recently, a new class of Fe-SC, the $Ae\text{AFe}_4\text{As}_4$ ($Ae =$ alkaline earth, $A = \text{K}, \text{Rb}, \text{Cs}$), was discovered [13]. In the $Ae\text{AFe}_4\text{As}_4$ family, Ae and A form alternating planes along the c axis, which distinguishes $Ae\text{AFe}_4\text{As}_4$ from the chemically substituted $(Ae_{0.5}A_{0.5})\text{Fe}_2\text{As}_2$, where Ae and A randomly occupy the same site (e.g., $\text{Ba}_{0.5}\text{K}_{0.5}\text{Fe}_2\text{As}_2$) [13]. Although these $Ae\text{AFe}_4\text{As}_4$ compounds were discovered in the polycrystalline form, single crystals of $\text{CaKFe}_4\text{As}_4$ were synthesized and investigated [14,15]. Pure, or undoped, $\text{CaKFe}_4\text{As}_4$ is superconducting below ~ 35 K without any other structural or magnetic phase transitions. Upon pressure

tuning up to ~ 6 GPa, the superconducting transition temperature T_c is weakly suppressed and a half-collapsed-tetragonal (hcT) transition that destroys bulk superconductivity is identified at ~ 4 GPa [16].

On one side, electron doping of $\text{CaKFe}_4\text{As}_4$ via Ni- or Co-substitution suppresses superconductivity and induces a new-type of antiferromagnetic order, the hedgehog-spin-vortex magnetic order that has no accompanying structural transition [17]. Pressure tuning of the Ni-substituted $\text{CaKFe}_4\text{As}_4$ up to ~ 5 GPa leads to a suppression of the T_N associated with the hedgehog-spin-vortex antiferromagnetic transition and a small local maximum in T_c located where $T_c(p)$ and $T_N(p)$ lines intersect and a hcT transition at ~ 4 GPa [18]. On the other side, a very recent study reports that nominal hole doping into $\text{CaKFe}_4\text{As}_4$ via Mn substitution also reveals a magnetic phase region as well as suppressing the superconducting transition temperature [19]. In the BaFe_2As_2 family, the effects of the transition metal substitution have been studied intensively and it is suggested that compared with Co- or Ni substitution, Mn behaves more local-moment-like. For example, solely Mn substitution could not induce superconductivity in BaFe_2As_2 as compared to Co or Ni substitution [6,20]. Mn substitution suppresses superconducting transition temperature more rapidly than Co or Ni [19,21].

The observation that Mn appears to behave more local-moment-like than Ni or Co [19] has its consequences for coexistence of superconductivity and magnetism in these materials. Whereas in Ni-substituted $\text{CaKFe}_4\text{As}_4$, the coexistence of SC and magnetism is fairly consistent with a simple model [22] in which SC and itinerant magnetism compete for the same electronic density of states [23,24]. In Mn-substituted $\text{CaKFe}_4\text{As}_4$, Mn appears to have local-moment-like behavior, so that simple model of Machida does not work any more, and, in part, the observed T_c suppression

*Present address: National High Magnetic Field Laboratory, Florida State University, Tallahassee, Florida 32310, USA; li.xiang@magnet.fsu.edu

[†]canfield@ameslab.gov

with Mn [19] is due to Abrikosov-Gor'kov mechanism [25]. So it appears that Mn-substituted $\text{CaKFe}_4\text{As}_4$ has enough significant differences with Ni (/Co) substituted ones to investigate the tunability of the magnetic phase and its interplay with superconductivity.

In this paper, we present a pressure study of $\text{CaK}(\text{Fe}_{1-x}\text{Mn}_x)_4\text{As}_4$ ($x = 0.024$) up to ~ 5 GPa. From resistance measurements, the superconducting transition temperature T_c and the magnetic transition temperature T_N were identified. A pressure-temperature ($p-T$) phase diagram is constructed accordingly. Upon increasing pressure, T_c first increases and then decreases with a maximum at ~ 2 GPa, whereas T_N is monotonically suppressed intersecting the $T_c(p)$ line at $p_c \sim 2$ GPa. Pressure-dependent resistance analysis also suggest a hcT transition at ~ 4.3 GPa. Furthermore, superconducting upper critical field analysis suggests a Fermi-surface reconstruction as well as a change in the pressure dependence of the superconducting coherence length at p_c .

II. EXPERIMENTAL DETAILS

Single crystals of $\text{CaK}(\text{Fe}_{1-x}\text{Mn}_x)_4\text{As}_4$ ($x = 0.024$) with sharp superconducting transitions at ambient pressure [see Figs. 1(b) and 2(b)] were grown using high-temperature solution growth [14,15]. The substitution level x was determined by performing Energy dispersive x-ray spectroscopy (EDS) [19]. The in-plane ab resistance was measured using the standard four-probe configuration. The $25 \mu\text{m}$ Pt wires were spot welded to the samples. Two samples, 1 and 2, were measured in a piston-cylinder cell (PCC) [26] and a modified Bridgman anvil cell (MBAC) [27], respectively. Pressure values for both cells, at low temperature, were inferred from the $T_c(p)$ of lead [28,29]. For the PCC, a 4:6 mixture of light mineral oil:n-pentane was used as the pressure medium, which solidifies, at room temperature, in the range of 3–4 GPa. For the MBAC, a 1:1 mixture of isopentane:n-pentane was used as the pressure medium, which solidifies, at room temperature, in the range of 6–7 GPa. Both of the solidification pressures are well above the maximum pressures achieved in the pressure cells, which suggests good hydrostatic conditions [30,31]. The ac resistance measurements were performed in a Quantum Design physical property measurement system (PPMS) using $I = 1$ mA; $f = 17$ Hz excitation, on cooling with a rate of 0.25 K/min, and the magnetic field was applied along the crystallographic c axis of the $\text{CaK}(\text{Fe}_{0.976}\text{Mn}_{0.024})_4\text{As}_4$ samples.

III. RESULTS AND DISCUSSION

Figures 1(a) and 2(a) present the temperature dependent resistance of $\text{CaK}(\text{Fe}_{0.976}\text{Mn}_{0.024})_4\text{As}_4$ sample 1 and 2 in a PCC under pressures up to 2.03 GPa and in a MBAC under pressures up to 5.15 GPa, respectively [Figs. 1(c) and 2(c)]. For both samples, at ambient pressure, resistance decreases upon cooling, showing metallic behavior. At ~ 30 K, a kink-like anomaly is observed and is associated with a magnetic transition T_N . At ~ 10 K, a sharp drop of resistance is observed [Figs. 1(b) and 2(b)] as the compound goes through the superconducting transition [19].

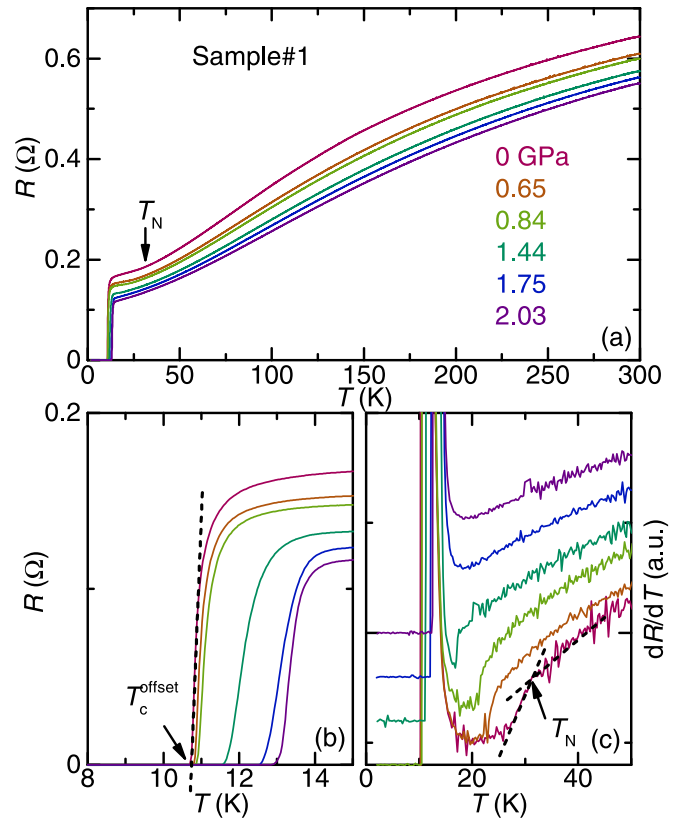


FIG. 1. (a) Evolution of the in-plane resistance with hydrostatic pressure up to 2.03 GPa measured in a piston-cylinder cell (PCC) for $\text{CaK}(\text{Fe}_{0.976}\text{Mn}_{0.024})_4\text{As}_4$, sample 1. (b) Enlarged view of the low-temperature resistance showing the superconducting transition. Criterion for T_c^{offset} is indicated by dashed line and arrow in the figure. (c) Temperature derivative of the resistance dR/dT showing the evolution of the magnetic transition T_N . Criterion for T_N is indicated by dashed lines and arrow in the figure.

Upon increasing pressure several changes take place. The normal-state resistance decreases and T_N and T_c change as shown in Figs. 1 and 2. As shown in the figures, T_c increases upon increasing pressure up to ~ 2 GPa. Further increasing of pressure suppresses T_c . In addition, the sharp superconducting transition at low pressures becomes broadened at higher pressures. For $p \geq 4.50$ GPa, the resistance does not drop to zero down the lowest temperature measured in this study (1.8 K).

To better trace the magnetic transition temperature T_N , the temperature derivative dR/dT is calculated and plotted in Figs. 1(c) and 2(c). It is seen that the kink-like anomaly in $R(T)$ is revealed as a step-like anomaly in dR/dT . As shown in the figures, T_N is suppressed by increasing pressure until it reaches the $T_c(p)$ line and is not resolved any more at higher pressures.

The pressure-dependent resistance at fixed temperatures for sample 2 is further analyzed and plotted in Fig. 3. Again, at all temperatures above superconducting transition, resistance decreases upon increasing pressure. In addition, a kink-like anomaly in the $R(p)$ curves is observed at a critical pressure $p^* \sim 4.3$ GPa. It is worth noting such a behavior is also observed in the parent and Ni-substituted $\text{CaKFe}_4\text{As}_4$ [16,18,32], where the anomaly is associated with

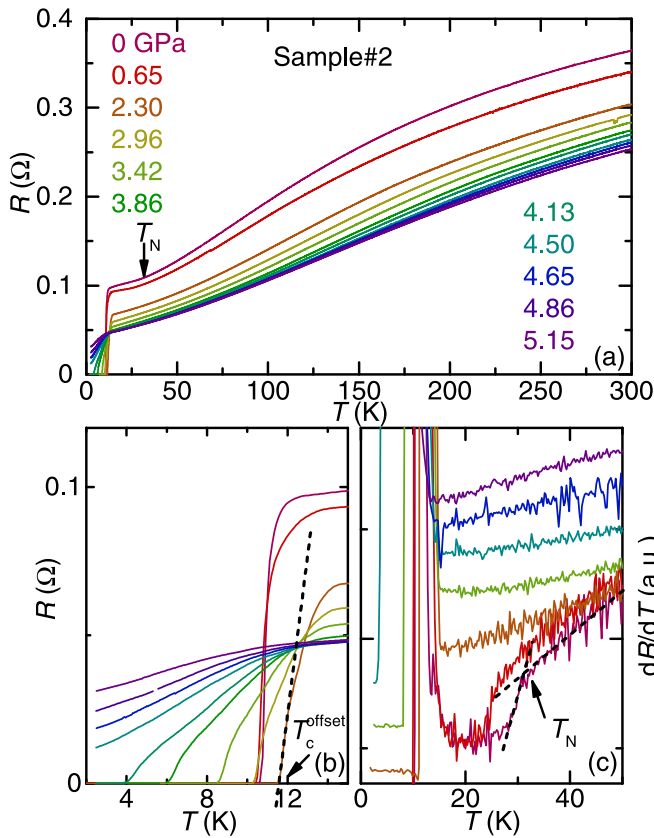


FIG. 2. (a) Evolution of the in-plane resistance with hydrostatic pressure up to 5.15 GPa measured in a modified Bridgman anvil cell (MBAC) for $\text{CaK}(\text{Fe}_{0.976}\text{Mn}_{0.024})_4\text{As}_4$, sample 2. (b) Enlarged view of the low-temperature resistance showing the superconducting transition. Criterion for T_c^{offset} is indicated by dashed line and arrow in the figure. (c) Temperature derivative of the resistance dR/dT showing the evolution of the magnetic transition T_N . Criterion for T_N is indicated by dashed lines and arrow in the figure.

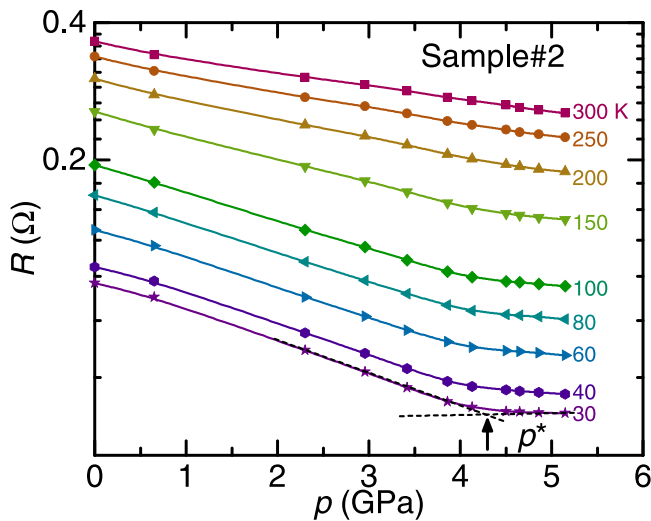


FIG. 3. Pressure dependence of the resistance, $R(p)$, at fixed temperatures for $\text{CaK}(\text{Fe}_{0.976}\text{Mn}_{0.024})_4\text{As}_4$ sample 2. The critical pressure p^* (indicated by dashed lines and arrow), which is associated with the hcT phase, is described in details in the text.

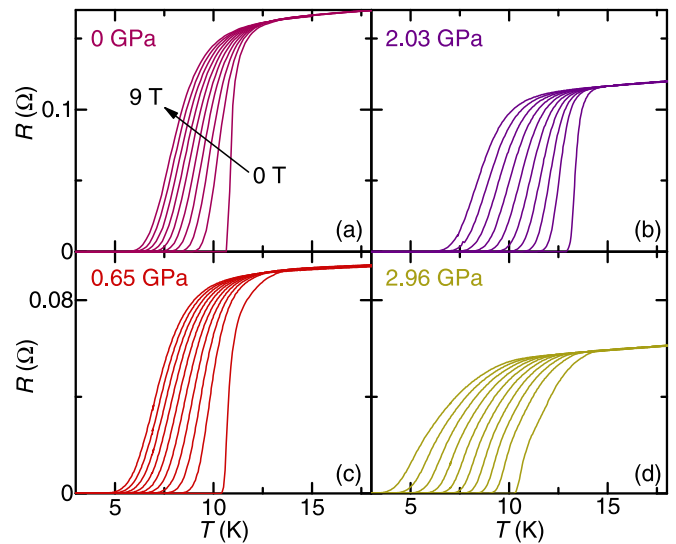


FIG. 4. Temperature dependence of resistance under magnetic field up to 9 T for selected pressures for $\text{CaK}(\text{Fe}_{0.976}\text{Mn}_{0.024})_4\text{As}_4$ sample 1 [(a),(b)] and sample 2 [(c),(d)].

a half-collapsed-tetragonal (hcT) phase transition at around 4–4.15 GPa. In the parent $\text{CaKFe}_4\text{As}_4$ compound, it is demonstrated that across the hcT transition, the As-As bonds forms across the Ca layer, which causes a sudden decrease in the c lattice parameter and an expansion in the a lattice parameter [16]. In addition such a collapsed tetragonal transition is often accompanied by significant changes of electronic properties, which can lead to the loss of superconductivity [16,33,34]. Based on the analogy, we identify this anomaly as an indication of the hcT transition that exists from base temperature up to at least 30 K. The superconducting transition for $p > p^*$ is likely not bulk, which could cause the broadening of the superconducting transition at high pressures as seen in Fig. 2(a) [16,18]. Similar hcT transitions are also predicted and observed in other $A\text{eAFe}_4\text{As}_4$ compounds [33]. Specifically, the hcT transition for $\text{CaRbFe}_4\text{As}_4$, $\text{RbEuFe}_4\text{As}_4$, and $\text{CsEuFe}_4\text{As}_4$ are experimentally shown to be ~ 6 GPa, ~ 10 GPa, and ~ 12 GPa [35,36]. Note that in the parent and Ni-substituted $\text{CaKFe}_4\text{As}_4$, the hcT transition remains around 4 GPa, demonstrating the insensitivity of the hcT transition pressure to Ni or Mn substitution.

The superconducting upper critical field H_{c2} can be evaluated from the $R(T)$ data taken at different applied magnetic fields and pressures, shown in Fig. 4 at pressures lower than p^* , where the superconductivity is believed to be bulk, using the offset criteria defined in Figs. 1 and 2. The temperature dependent H_{c2} under pressures up to 3.86 GPa is presented in Fig. 5. As shown in the figure, H_{c2} is linear in temperature except for magnetic fields below 1 T. This curvature at low magnetic fields has been also observed in other FeSC and can be explained by the multiband nature of superconductivity [37–40]. In addition, it is observed that the evolution of the temperature-dependent H_{c2} with pressure is nonmonotonic.

The evolution of the superconducting and the magnetic transition temperatures with pressure is summarized in a pressure-temperature phase diagram presented in Fig. 6. T_c^{offset} and T_N values are obtained using the criteria defined

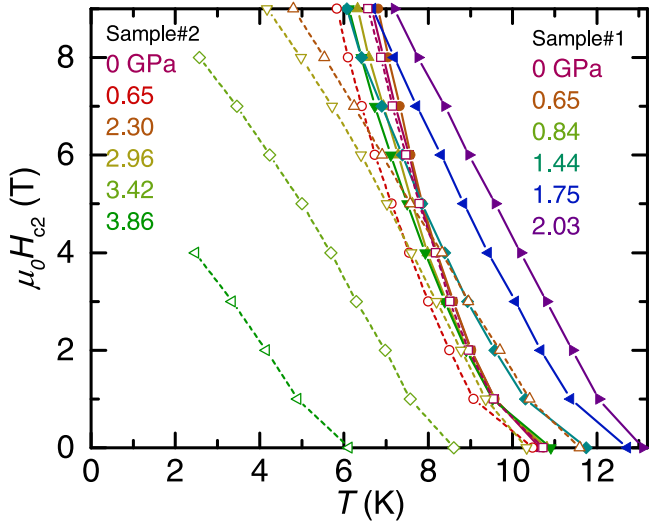


FIG. 5. Temperature dependence of the superconducting upper critical field $H_{c2}(T)$ under selected pressures for $\text{CaK}(\text{Fe}_{0.976}\text{Mn}_{0.024})_4\text{As}_4$. T_c^{offset} is used. Solid and open symbols are two samples measured in PCC and MBAC, respectively.

in Figs. 1 and 2 and the hcT phase above p^* is indicated by the blue dotted line in the figure. We see that for $\text{CaK}(\text{Fe}_{0.976}\text{Mn}_{0.024})_4\text{As}_4$, upon increasing pressure from 0 to ~ 1.5 GPa, T_N is monotonically suppressed from 30 K to 18 K. In terms of the superconducting transition temperatures, T_c^{offset} first increases from 10 K to 13 K with pressure increasing from 0 to 2.03 GPa. Upon further increasing pressure to 4.13 GPa, T_c^{offset} is suppressed to 3.9 K, resulting in a local maximum in T_c at ~ 2 GPa. Above $p^* \sim 4.3$ GPa, $\text{CaK}(\text{Fe}_{0.976}\text{Mn}_{0.024})_4\text{As}_4$ enters into the hcT phase at low temperatures. The pressure-temperature phase diagram of $\text{CaK}(\text{Fe}_{0.976}\text{Mn}_{0.024})_4\text{As}_4$ is qualitatively similar to that of $\text{CaK}(\text{Fe}_{1-x}\text{Ni}_x)_4\text{As}_4$ ($x = 0.033, 0.05$) [18]. For all three compounds, The $T_N(p)$ and $T_c(p)$ lines intersect at the maximum T_c point of the $T_c(p)$ curve. Note that below we call this intersect-pressure p_c [identified by a sharp minima in the $-(1/T_c)(d\mu_0 H_{c2}/dT)|_{T_c}$ data] [18]. Quantitatively, the suppression of T_N with p is faster for Mn substitution, compared with that for Ni substitution (the initial suppression of T_N is ~ 8 K/GPa for Mn substitution, ~ 3.3 K/GPa and ~ 6.5 K/GPa for Ni substitution $x = 0.033$ and 0.05 , correspondingly). In addition, p_c for Mn substitution (~ 2 GPa) is lower than that of Ni substitution (~ 3 GPa for $x=0.033$ and 0.05) [18]. Such nonmonotonic behavior of T_c under pressure could be qualitatively understood as a result of coexistence of itinerant magnetism and superconductivity that are competing in the same, shared, electron subsystem [22–24].

The superconducting upper critical field H_{c2} was further analyzed following Refs. [18,38,39,41]. Generally speaking, the slope of the upper critical field normalized by T_c is related to the Fermi velocity and superconducting gap of the system [37]. In the clean limit for a single band case,

$$-(1/T_c)(d\mu_0 H_{c2}/dT)|_{T_c} \propto 1/v_F^2 \quad (1)$$

where v_F is the Fermi velocity. Even though the superconductivity in $\text{CaKFe}_4\text{As}_4$ is multiband, Eq. (1) can give

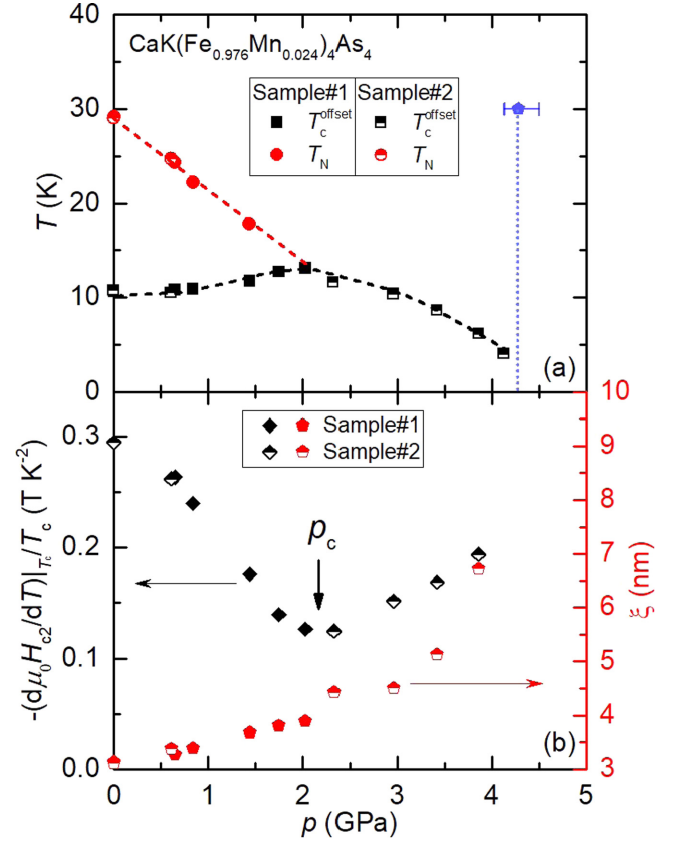


FIG. 6. (a) Pressure-temperature phase diagram of $\text{CaK}(\text{Fe}_{0.976}\text{Mn}_{0.024})_4\text{As}_4$ as determined from resistance measurements. The squares and circles represent the superconducting T_c^{offset} and magnetic T_N phase transitions. The blue-dotted line indicates the half-collapsed tetragonal phase transition up to 30 K, inferred from the pressure-dependent resistance $R(p)$ data in Fig. 3. (b) Pressure dependence of the normalized upper critical field slope $-(1/T_c)(d\mu_0 H_{c2}/dT)|_{T_c}$ (black symbols) and inferred coherence length ξ (red symbols). A local minimum in the slope and a clear change of the coherence length at p_c (indicated by the arrow) are observed near the pressure where $T_c^{\text{offset}}(p)$ and $T_N(p)$ lines intersect.

qualitative insight into changes induced by pressure. As shown in Fig. 6(b), upon increasing pressure, the normalized slope of the upper critical field $-(1/T_c)(d\mu_0 H_{c2}/dT)|_{T_c}$ [the slope $d\mu_0 H_{c2}/dT|_{T_c}$ is calculated by linear fitting the $H_{c2}(T)$ data above 1 T in Fig. 5] first decreases and then increases, resulting a minimum of $-(1/T_c)(d\mu_0 H_{c2}/dT)|_{T_c}$ at p_c in the studied pressure range. In addition, p_c coincide with the cross of the $T_N(p)$ and $T_c(p)$ lines. Note that similar upper-critical-field behavior is also observed in the Ni-substituted $\text{CaK}(\text{Fe}_{1-x}\text{Ni}_x)_4\text{As}_4$ [18].

Coherence length ξ can be estimated from $|dH_{c2}^{\parallel c}/dT| = \phi_0/2\pi\xi_{\perp}^2 T_c$, where ϕ_0 is the magnetic flux quantum, ξ_{\perp} is the effective Ginzburg-Landau coherence length near T_c [19,42] when magnetic field is applied perpendicular to the ab plane. As shown in the figure, ξ monotonically increases with increasing pressure. In addition, $\xi(p)$ shows a sudden increase at p_c . This is not surprising

as coherence length ξ is also inferred from the upper critical field slope dH_{c2}/dT .

The clear changes in the pressure dependence of normalized slope upper critical field slope, $-(1/T_c)(d\mu_0 H_{c2}/dT)|_{T_c}$, and in coherence length ξ coincides with the pressure p_c across which T_N is suppressed below T_c . We argue that this indicates a possible Fermi-surface reconstruction, which could happen due to the pressure-induced disappearance of magnetism, which is also observed in the BaFe_2As_2 family [18,43–46].

IV. CONCLUSIONS

In summary, the resistance of the Mn-substituted iron-based superconductor $\text{CaK}(\text{Fe}_{1-x}\text{Mn}_x)_4\text{As}_4$ ($x = 0.024$) was investigated under hydrostatic pressures up to 5.15 GPa and in magnetic fields up to 9 T. It is observed that the magnetic transition temperature T_N is suppressed upon increasing pressure, whereas the superconducting transition temperature exhibits a nonmonotonic dependence on pressure with a maximum at ~ 2 GPa in the studied pressure range. $\text{CaK}(\text{Fe}_{1-x}\text{Mn}_x)_4\text{As}_4$ ($x = 0.024$) likely goes through a half-collapsed-tetragonal phase transition when pressure is increased across ~ 4.3 GPa. A minimum in the normalized slope of the upper critical field, $-(1/T_c)(d\mu_0 H_{c2}/dT)|_{T_c}$, and a sudden change of the

coherence length ξ are observed at a pressure where $T_N(p)$ and $T_c(p)$ lines intersect. This suggests a possible Fermi-surface reconstruction associated with the disappearance of the magnetism.

The results of these studies show that there is no obvious or qualitative difference in the pressure response between Ni- and Mn-substituted $\text{CaKFe}_4\text{As}_4$. The observation of lower value of p_c in Mn-substituted $\text{CaKFe}_4\text{As}_4$ is, at least in part, due to lower T_N at ambient pressure. We do not see unambiguous, additional contribution from AG pair-breaking to the evolution of T_c under pressure, in contrast to the results on borocarbides [47,48], but in agreement with the behavior of Gd-substituted La_3In [49]. As such then, the pressure dependent phase diagram for the Mn-substituted $\text{CaKFe}_4\text{As}_4$ provides a full set of benchmarks that any theory trying to understand these materials would need to accommodate.

ACKNOWLEDGMENTS

This work is supported by the U.S. DOE, Basic Energy Sciences, Materials Science and Engineering Division under Contract No. DE-AC02-07CH11358. L.X. was supported by the Gordon and Betty Moore Foundation's EPIQS Initiative through Grant No. GBMF4411 and, in part, by the W. M. Keck Foundation.

-
- [1] Y. Kamihara, T. Watanabe, M. Hirano, and H. Hosono, *J. Am. Chem. Soc.* **130**, 3296 (2008).
- [2] H. Takahashi, K. Igawa, K. Arii, Y. Kamihara, M. Hirano, and H. Hosono, *Nature (London)* **453**, 376 (2008).
- [3] M. Rotter, M. Tegel, and D. Johrendt, *Phys. Rev. Lett.* **101**, 107006 (2008).
- [4] Z. A. Ren, G. C. Che, X. L. Dong, J. Yang, W. Lu, W. Yi, X. L. Shen, Z. C. Li, L. L. Sun, F. Zhou *et al.*, *Europhys. Lett.* **83**, 17002 (2008).
- [5] J. Paglione and R. L. Greene, *Nat. Phys.* **6**, 645 (2010).
- [6] P. C. Canfield and S. L. Bud'ko, *Annu. Rev. Condens. Matter Phys.* **1**, 27 (2010).
- [7] D. C. Johnston, *Adv. Phys.* **59**, 803 (2010).
- [8] P. Dai, *Rev. Mod. Phys.* **87**, 855 (2015).
- [9] M. S. Torikachvili, S. L. Bud'ko, N. Ni, and P. C. Canfield, *Phys. Rev. B* **78**, 104527 (2008).
- [10] S. A. J. Kimber, A. Kreyssig, Y.-Z. Zhang, H. O. Jeschke, R. Valentí, F. Yokaichiya, E. Colombier, J. Yan, T. C. Hansen, T. Chatterji *et al.*, *Nat. Mater.* **8**, 471 (2009).
- [11] S. Avci, O. Chmaissem, D. Y. Chung, S. Rosenkranz, E. A. Goremychkin, J. P. Castellán, I. S. Todorov, J. A. Schlueter, H. Claus, A. Daoud-Aladine *et al.*, *Phys. Rev. B* **85**, 184507 (2012).
- [12] J. J. Wu, J.-F. Lin, X. C. Wang, Q. Q. Liu, J. L. Zhu, Y. M. Xiao, P. Chow, and C. Jin, *Proc. Natl. Acad. Sci. U.S.A.* **110**, 17263 (2013).
- [13] A. Iyo, K. Kawashima, T. Kinjo, T. Nishio, S. Ishida, H. Fujihisa, Y. Gotoh, K. Kihou, H. Eisaki, and Y. Yoshida, *J. Am. Chem. Soc.* **138**, 3410 (2016).
- [14] W. R. Meier, T. Kong, U. S. Kaluarachchi, V. Taufour, N. H. Jo, G. Drachuck, A. E. Böhmer, S. M. Saunders, A. Sapkota, A. Kreyssig *et al.*, *Phys. Rev. B* **94**, 064501 (2016).
- [15] W. R. Meier, T. Kong, S. L. Bud'ko, and P. C. Canfield, *Phys. Rev. Mater.* **1**, 013401 (2017).
- [16] U. S. Kaluarachchi, V. Taufour, A. Sapkota, V. Borisov, T. Kong, W. R. Meier, K. Kothapalli, B. G. Ueland, A. Kreyssig, R. Valenti, R. J. McQueeney, A. I. Goldman, S. L. Budko, and P. C. Canfield, *Phys. Rev. B* **96**, 140501(R) (2017).
- [17] W. R. Meier, Q.-P. Ding, A. Kreyssig, S. L. Bud'ko, A. Sapkota, K. Kothapalli, V. Borisov, R. Valentí, C. D. Batista, P. P. Orth *et al.*, *npj Quantum Mater.* **3**, 5 (2018).
- [18] L. Xiang, W. R. Meier, M. Xu, U. S. Kaluarachchi, S. L. Bud'ko, and P. C. Canfield, *Phys. Rev. B* **97**, 174517 (2018).
- [19] M. Xu, J. Schmidt, E. Gati, L. Xiang, W. R. Meier, V. G. Kogan, S. L. Bud'ko, and P. C. Canfield, *Phys. Rev. B* **105**, 214526 (2022).
- [20] A. Thaler, H. Hodovanets, M. S. Torikachvili, S. Ran, A. Kracher, W. Straszheim, J. Q. Yan, E. Mun, and P. C. Canfield, *Phys. Rev. B* **84**, 144528 (2011).
- [21] J. Li, Y. F. Guo, S. B. Zhang, J. Yuan, Y. Tsujimoto, X. Wang, C. I. Sathish, Y. Sun, S. Yu, W. Yi *et al.*, *Phys. Rev. B* **85**, 214509 (2012).
- [22] K. Machida, *J. Phys. Soc. Jpn.* **50**, 2195 (1981).
- [23] S. L. Bud'ko, V. G. Kogan, R. Prozorov, W. R. Meier, M. Xu, and P. C. Canfield, *Phys. Rev. B* **98**, 144520 (2018).
- [24] A. Kreyssig, J. M. Wilde, A. E. Böhmer, W. Tian, W. R. Meier, B. Li, B. G. Ueland, M. Xu, S. L. Bud'ko, P. C. Canfield, R. J. McQueeney, and A. I. Goldman, *Phys. Rev. B* **97**, 224521 (2018).
- [25] A. A. Abrikosov and L. P. Gor'kov, *Z. Eksp. Teor. Fiz.* **39** (1960).
- [26] S. L. Bud'ko, A. N. Voronovskii, A. G. Gapotchenko, and E. S. Itskevich, *Zh. Eksp. Teor. Fiz.* **86**, 778 (1984).

- [27] E. Colombier and D. Braithwaite, *Rev. Sci. Instrum.* **78**, 093903 (2007).
- [28] B. Bireckoven and J. Wittig, *J. Phys. E* **21**, 841 (1988).
- [29] L. Xiang, E. Gati, S. L. Bud'ko, R. A. Ribeiro, A. Ata, U. Tutsch, M. Lang, and P. C. Canfield, *Rev. Sci. Instrum.* **91**, 095103 (2020).
- [30] S. K. Kim, M. S. Torikachvili, E. Colombier, A. Thaler, S. L. Bud'ko, and P. C. Canfield, *Phys. Rev. B* **84**, 134525 (2011).
- [31] M. S. Torikachvili, S. K. Kim, E. Colombier, S. L. Bud'ko, and P. C. Canfield, *Rev. Sci. Instrum.* **86**, 123904 (2015).
- [32] E. Gati, L. Xiang, S. L. Bud'ko, and P. C. Canfield, *Ann. Phys.* **532**, 2000248 (2020).
- [33] V. Borisov, P. C. Canfield, and R. Valentí, *Phys. Rev. B* **98**, 064104 (2018).
- [34] E. Gati, S. Köhler, D. Guterding, B. Wolf, S. Knöner, S. Ran, S. L. Bud'ko, P. C. Canfield, and M. Lang, *Phys. Rev. B* **86**, 220511(R) (2012).
- [35] R. L. Stillwell, X. Wang, L. Wang, D. J. Campbell, J. Paglione, S. T. Weir, Y. K. Vohra, and J. R. Jeffries, *Phys. Rev. B* **100**, 045152 (2019).
- [36] D. E. Jackson, D. VanGennep, W. Bi, D. Zhang, P. Materne, Y. Liu, G.-H. Cao, S. T. Weir, Y. K. Vohra, and J. J. Hamlin, *Phys. Rev. B* **98**, 014518 (2018).
- [37] V. G. Kogan and R. Prozorov, *Rep. Prog. Phys.* **75**, 114502 (2012).
- [38] U. S. Kaluarachchi, V. Taufour, A. E. Böhmer, M. A. Tanatar, S. L. Bud'ko, V. G. Kogan, R. Prozorov, and P. C. Canfield, *Phys. Rev. B* **93**, 064503 (2016).
- [39] L. Xiang, U. S. Kaluarachchi, A. E. Böhmer, V. Taufour, M. A. Tanatar, R. Prozorov, S. L. Bud'ko, and P. C. Canfield, *Phys. Rev. B* **96**, 024511 (2017).
- [40] D. Mou, T. Kong, W. R. Meier, F. Lochner, L.-L. Wang, Q. Lin, Y. Wu, S. L. Bud'ko, I. Eremin, D. D. Johnson *et al.*, *Phys. Rev. Lett.* **117**, 277001 (2016).
- [41] V. Taufour, N. Foroozani, M. A. Tanatar, J. Lim, U. Kaluarachchi, S. K. Kim, Y. Liu, T. A. Lograsso, V. G. Kogan, R. Prozorov, S. L. Bud'ko, J. S. Schilling, and P. C. Canfield, *Phys. Rev. B* **89**, 220509(R) (2014).
- [42] A. Gurevich, *Rep. Prog. Phys.* **74**, 124501 (2011).
- [43] G. Liu, H. Liu, L. Zhao, W. Zhang, X. Jia, J. Meng, X. Dong, J. Zhang, G. F. Chen, G. Wang *et al.*, *Phys. Rev. B* **80**, 134519 (2009).
- [44] J. Dai, Q. Si, J.-X. Zhu, and E. Abrahams, *Proc. Natl. Acad. Sci. U.S.A.* **106**, 4118 (2009).
- [45] C. Liu, T. Kondo, R. M. Fernandes, A. D. Palczewski, E. D. Mun, N. Ni, A. N. Thaler, A. Bostwick, E. Rotenberg, J. Schmalian *et al.*, *Nat. Phys.* **6**, 419 (2010).
- [46] C. Liu, A. D. Palczewski, R. S. Dhaka, T. Kondo, R. M. Fernandes, E. D. Mun, H. Hodovanets, A. N. Thaler, J. Schmalian, S. L. Bud'ko, P. C. Canfield, and A. Kaminski, *Phys. Rev. B* **84**, 020509(R) (2011).
- [47] H. Michor, M. El-Hagary, L. Naber, E. Bauer, and G. Hilscher, *Phys. Rev. B* **61**, R6487 (2000).
- [48] J.-H. Choi, H. Doh, E.-M. Choi, S.-I. Lee, M. Ohashi, and N. Môri, *Phys. Rev. B* **65**, 024520(R) (2001).
- [49] M. B. Maple and K.-S. Kim, *Phys. Rev. Lett.* **23**, 118 (1969).